[Ag₄₈(C≡C^tBu)₂₀(CrO₄)₇]: An Atomically Precise Silver Nanocluster Co-Protected by Inorganic and Organic Ligands

Shan-Shan Zhang,† Fahri Alkan,‡ Hai-Feng Su,§ Christine M. Aikens,*,‡ Chen-Ho Tung,† and Di Sun*,†

*Key Laboratory of Colloid and Interface Chemistry, Ministry of Education, School of Chemistry and Chemical Engineering, State Key Laboratory of Crystal Materials, Shandong University, Jinan, 250100, People's Republic of China.

Department of Chemistry, Kansas State University, Manhattan, Kansas 66506, USA.

§State Key Laboratory for Physical Chemistry of Solid Surfaces and Department of Chemistry, College of Chemistry and Chemical Engineering, Xiamen University, Xiamen, 361005, People's Republic of China.

ABSTRACT: The elaborate selection of the capping ligands is of great importance in the synthesis of atomically precise metal nanoclusters. Organic thiolates, alkynyls, phosphines and/or their combinations are the most widely utilized to protect metal nanoclusters, while inorganic oxo anions have been almost neglected in this field. Herein, the first $CrO_4^{2-}/^{1}BuC\equiv C^{-}$ co-capped Ag_{48} nanocluster (**SD/Ag48**) was synthesized and structurally characterized by single-crystal X-ray diffraction (SCXRD). The *pseudo*-fivefold symmetric metal skeleton of **SD/Ag48** shows a core-shell structure comprised of an Ag_{23} cylinder encircled by an outer Ag_{25} shell. Unprecedentedly, co-existence of inorganic (CrO_4^{2-}) and organic ($BuC\equiv C^{-}$) ligands was observed on the surface of **SD/Ag48**. The inorganic CrO_4^{2-} anion plays three important roles in the construction of silver nanoclusters: i) passivating the Ag_{23} kernel; ii) connecting the core and shell; and iii) protecting the Ag_{25} shell. This nanocluster belongs to a 14e superatom system and exhibits successive molecule-like absorption bands from the visible to the ultraviolet region. This work not only establishes a fresh inorganic ligand strategy in the synthesis of silver nanoclusters but also provides a new insight about the important surface coordination chemistry of CrO_4^{2-} in the shape-control of silver nanoclusters.

INTRODUCTION

Ligand-protected metal nanoclusters (e.g. copper, silver, gold and their alloys) with precise numbers of metal atoms and definite composition of ligand coatings have attracted extensive attention in recent years due to their unique bridging role between atoms and plasmonic nanoparticles, and promising optical and physicochemical properties. For a long time, the synthesis of metal nanoparticles has been dominated by polydispersity² which is not desirable, because their unique properties mainly depended on their size and shape. However, precise control over the compositions including those of the metallic kernel and the ligand shell to realize monodispersity at atomic precision is still one of the biggest challenges in the field. The earliest experimental breakthrough in X-ray structure of gold nanoclusters was achieved for Au₁₀₂³ and the ability to crystallize these compounds is closely related to their high stability. Since then, a large number of gold nanoclusters with well-resolved atomiclevel structures have sprung up4 and the largest known to date is Au_{246.5} Compared to gold nanoclusters, the silver counterparts, however, are still largely lagging which is mainly due to their relatively low stability. Up to date, only limited fully characterized silver nanoclusters have been reported such as Ag₂₁,⁶ Ag_{23} , $^7Ag_{25}$, $^8Ag_{29}$, $^9Ag_{34}$, $^{10}Ag_{44}$, $^{11}Ag_{46}$, $^{12}Ag_{50}$, $^{13}Ag_{62}$, $^{14}Ag_{67}$, $^{15}Ag_{74}$, $^{16}Ag_{141}$, $^{17}Ag_{146}$, $^{18}Ag_{206}$, $^{19}Ag_{210}$, 20 and currently the largest Ag₃₇₄.²¹

Considering their assembly, the capping ligand is one of the most important factors that dictates the final structures as well as their related properties.²² Thus, engineering the surface ligands of metal nanoclusters is an easy-to-use strategy to control

the metallic kernels as well as the ligand shell. The most widely used capping organic ligands are thiolates, alkynyls, phosphines and/or their combinations, while inorganic ligands have been limited to halogens or chalcogens. Of note, all these ligands coordinate to surface of nanoclusters using only one or two atoms (P, S, or C atom) with mono- or multidentate bridging modes, which is not favorable to their stability. In contrast, an inorganic oxo anion with polyatom backbone can act as a multisite and multidentate coordination scaffold to construct stable metal nanoclusters. However, no reports with inorganic oxo anions as ligands appeared in this field until now. Using such inorganic oxo anions, for example CrO_4^{2-} , MoO_4^{2-} , and WO_4^{2-} , will provide new opportunities to explore the synthesis of innovative metal nanoclusters.

Scheme 1. Synthetic Route for **SD/Ag48**. TMEDA = N,N,N',N'-Tetramethylethylenediamine.



Given the special coordinative advantages of inorganic oxo anions as one of the capping ligands and inspired by our previous work on inorganic oxo anion templated Ag(I) clusters, ²⁴ we firstly introduced these inorganic oxo anions into the synthesis of reduced silver nanoclusters and successfully isolated a novel $CrO_4^{2-}/BuC\equiv C^-$ co-capped Ag_{48} nanocluster (**SD/Ag48**). The

overall composition of this nanocluster was determined to be $[Ag_{48}(C\equiv C'Bu)_{20}(CrO_4)_7]$ containing 48 Ag atoms that can be divided into an inner Ag_{23} cylindrical kernel and outer Ag_{25} shell. Two CrO_4^{2-} anions at the two poles and five additional chromates on the equator region passivate the Ag_{23} cylinder. Twenty 'BuC $\equiv C^-$ ligands cap the surface of the Ag_{25} shell in a four-ring fashion with each ring having five 'BuC $\equiv C^-$ ligands. This is the first example of a silver nanocluster with both inorganic oxo anions and organic ligands capping the surface.

RESULTS AND DISCUSSION

Synthesis

The SD/Ag48 was synthesized by the reduction of a mixture of 'BuC≡CAg, K2Cr2O7, glutaric acid and Ag2O in CH3OH using NaBH₄ as a reductant at room temperature. Then, solvothermal treatment for the above mixture was performed at 70 °C (Scheme 1). The final yield is moderate (~45 %) and the repeatability of the synthesis experiment is quite good. The black crystals of SD/Ag48 were grown by solvent evaporation of filtrate after solvothermal reaction at room temperature. The pure sample was collected as crystals by filtration. The solvothermal reaction is quite crucial for the formation of SD/Ag48 and no any crystalline products can be formed without such treatment. Although the glutaric acid is not found in **SD/Ag48**, it also plays important roles in assembly of SD/Ag48 such as adjusting pH value and dissolving Ag₂O. The SD/Ag48 was fully characterized by a series of spectroscopic, crystallographic and computational characterization techniques. The synthetic details and some basic characterizations such as powder X-ray diffraction, infrared spectra, UV-Vis spectra, cyclic voltammetry and so on are shown in the Supporting Information (SI)

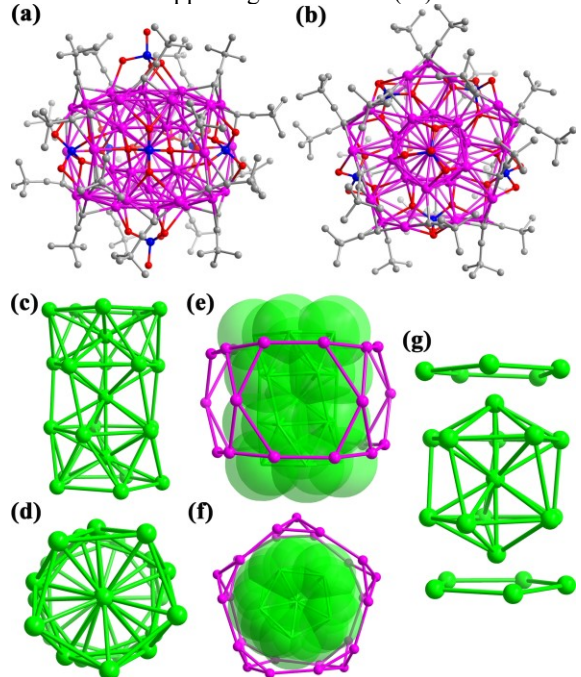


Figure 1. The side (a) and top (b) view of total molecular structure of **SD/Ag48**. (b) The side (c) and top (d) view of the Ag_{23} cylinder. The structure of $Ag_{23}@Ag_{25}$ viewed in two different (e) and (f) perspectives. (g) The formation of the Ag_{25} shell by capping two silver pentagons on the Ag_{13} Ino decahedron the top and bottom. (Color legend: Ag: purple and green; Cr: blue; C: gray; O: red).

X-ray Structure of Ag₄₈(C≡C^tBu)₂₀(CrO₄)₇ (SD/Ag48)

As revealed by SCXRD, SD/Ag48 crystallized in the triclinic P-1 space group and has a pseudo-fivefold symmetric drum-like shape (Figure 1a and 1b) with a height and diameter of 0.8 and 1.1 nm, respectively, excluding the ligand shell. The asymmetric unit of SD/Ag48 contains two complete molecules with identical chemical composition for each. The precise formula of **SD/Ag48** was identified as $[Ag_{48}(C \equiv C'Bu)_{20}(CrO_4)_7]$. The metallic skeleton of 48 silver atoms shows a particle-in-a-cylinder feature comprised of an Ag₂₃ cylinder (Figure 1c and 1d) encircled by an outer Ag₂₅ shell (Figure 1e and 1f), thus the best formula for describing this metallic kernel is Ag₂₃@Ag₂₅. The inner Ag23 cylinder can be seen as a central Ino decahedral Ag13 capped by two Ag₅ pentagons at the top and bottom in a staggered fashion (Figure 1g). The Ino decahedral Ag₁₃ consists of two Ag7 decahedra fused together by sharing one apical Ag atom in a nearly eclipsed conformation (torsion angles = 14~15° Figure S1). We also show the calculated Hirshfeld charges of silver atoms in the cluster in Figure S2. This analysis is in agreement with the Ag₂₃@Ag₂₅ formulation of the kernel as well.

The Ag···Ag distances in the Ag₂₃ cylinder fall in the range of 2.7221(13)-3.0372(14) Å, similar to the distances in bulk silver and related silver nanoclusters.²⁵ Of note, a kernel of 13 metal atoms is well known in Ag and Au nanoclusters,²⁶ but most cases involve the M₁₃ icosahedron, cuboctahedron and anticuboctahedron.²⁷ Although the 13-Au atom Ino decahedron has been observed in Au₁₃₀,²⁸ such special decahedron of 13-Ag atoms with in Ag₂₃ cylinder is very seldom. Alternatively, the Ag₂₃ cylinder can be seen as two classic Ag₁₃ icosahedra connected by sharing one apical Ag atom (Ag1) but missing two vertexes at two pole sites (Figure S3).

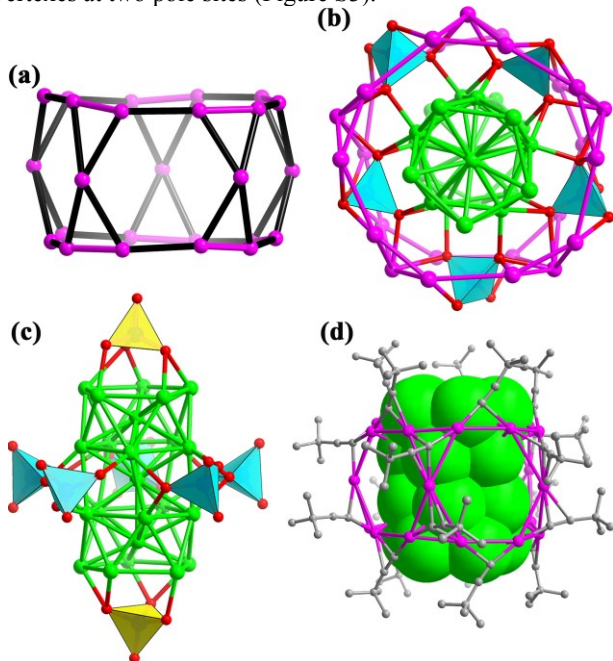


Figure 2. (a) Side view of the drum-like Ag_{25} shell. (b) Top view of coordination of five equatorial CrO_4^{2-} anions linking the Ag_{23} cylinder and Ag_{25} shell. (c) Full coordination of seven CrO_4^{2-} anions on the Ag_{23} cylinder. (d) Side view of the Ag_{23} cylinder encircled by the outer $Ag_{25}(C \equiv C'Bu)_{20}$ shell. (Color legend: Ag: purple and green; C: gray; O: red; CrO_4^{2-} : cyan or yellow tetrahedra).

Encircling the inner Ag_{23} cylinder is an Ag_{25} shell in a concentric fashion along the quasi-5-fold axis. The 25 Ag atoms in

the shell are organized in a three-ring manner with the number of silver atoms in each being 10, 5, and 10 (Figure S4). In a polyhedral view, the Ag₂₅ shell contains 10 trigons and 5 hexagons (Figure S5). The overall shape of the Ag₂₅ shell looks like a drum. There are five vertex-shared hexagonal windows (black hexagons in Figure 2a) on the drum body of the Ag₂₅ shell. Five equatorial CrO₄²⁻ anions penetrate them to coordinate on five tetragonal faces of the inner Ag23 cylinder and five hexagonal windows of the Ag₂₅ shell using $\mu_8 - \kappa^1 : \kappa^1 : \kappa^3 : \kappa^3$, $\mu_9 - \kappa^1 : \kappa^2 : \kappa^3 : \kappa^3$ and μ_{10} - κ^2 : κ^3 : κ^3 modes (cyan tetrahedra in Figure 2b), while the other two μ_5 - κ^1 : κ^2 : κ^2 CrO₄²- anions cap the apical pentagons at two poles of the Ag₂₃ cylinder (yellow tetrahedra in Figure 2c). The Ag-O bond lengths fall in the range of 2.263(9)-2.780(9) Å. The unique coordination of the inorganic CrO₄²- anion was found to have three important roles in the construction of SD/Ag48: i) passivating the Ag23 kernel; ii) connecting the core and shell; and iii) protecting the Ag₂₅ shell. All 20 'BuC≡C ligands adopt the μ_3 mode to cap the Ag₂₅ shell (Figure 2d and Figure S6a), connecting it to the Ag₂₃ cylinder (Ag-C: 2.064(15)-2.497(14) Å). Although every 'BuC≡C' ligand is ligated to three silver atoms, the detailed coordination modes of them are still different due to the diverse combinations of σ and π coordination fashions. Figure S6b shows the coordination modes of both inorganic and organic ligands in a more detailed fashion. The Ag···Ag distances in the Ag₂₅ shell are 2.8804(14)-3.4339(13) Å, and the distances between the Ag₂₃ cylinder and the Ag₂₅ shell fall in the range of 2.8885(14)-3.4067(13) Å, which consolidate the overall metallic skeleton of SD/Ag48.

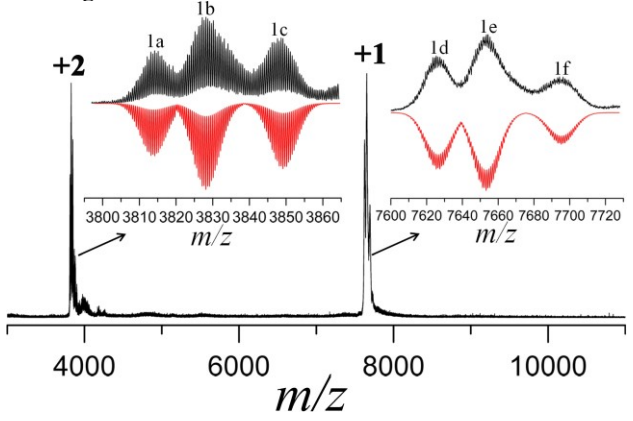


Figure 3. Positive ion mode ESI-MS of the crystals of **SD/Ag48** dissolved in CH₂Cl₂. Inset: The zoom-in ESI-MS of experimental (black line) and simulated (red line) for each labeled species.

Mass Spectroscopy and Solution Stability

As shown in Figure 3, the positive-ion ESI-MS of SD/Ag48 dissolved in dichloromethane shows two grouped signals, corresponding to +2 and +1 species, in the m/z range of 3000-11000. After carefully matching experimental mass spectra with calculated isotope distributions, we can identify each envelope containing three different species. The envelope in the m/z range of 3000-5000 is doubly charged species (1a-1c), and the most abundant species in this envelope is 1b centered at m/z3828.1455. corresponding to $[KAg_{48}(^{t}BuC\equiv C)_{19}(CrO_{4})_{7}(CH_{3}OH)(H_{2}O)_{3}]^{2+}$ (Calcd. 3828.1211), which corresponds to the SD/Ag48 losing a 'BuC≡C⁻ ligand and adding a K⁺ ion. Similarly, 1c was assigned to [KAg₄₈('BuC≡C)₁₉(CrO₄)₇]²⁺ species. 1a is formed by losing

one 'BuC≡CAg and adding two K⁺ ions from the parent SD/Ag48. In another envelope, the predominant peak 1e cenm/zassigned at 7653.3160 is $[NaAg_{48}(^{t}BuC \equiv C)_{20}(CrO_{4})_{7}(H_{2}O)]^{+}$ (Calcd. 7653.2922), which can be seen as the molecular ion peak of SD/Ag48 adding one Na⁺ and H₂O. **1d** and **1f** are formed by losing one 'BuC≡CAg and one 'BuC≡C- ligand from the pristine SD/Ag48 when dissolved in CH₂Cl₂, respectively. All the formulae of these species are listed in Table S1. These results clearly demonstrate that **SD/Ag48** can remain intact in CH₂Cl₂. More importantly, combined with the solid-state structure analysis of SD/Ag48, we can clearly determine that SD/Ag48 is a neutral nanocluster.

Optical Properties and DFT Calculations

As shown in Figure 4a, the CH₂Cl₂ solution of the **SD/Ag48** shows highly structured absorption bands including two weak peaks at 309 and 397 nm, and one prominent absorption peak at 491 nm. Moreover, the **SD/Ag48** remained stable at room temperature in CH₂Cl₂ at least 5 days (Figure S7). The molecule-like optical absorption originates from interband electronic transitions between discrete energy levels. The optical energy gap is determined to be 1.09 eV (Figure 4a, inset).

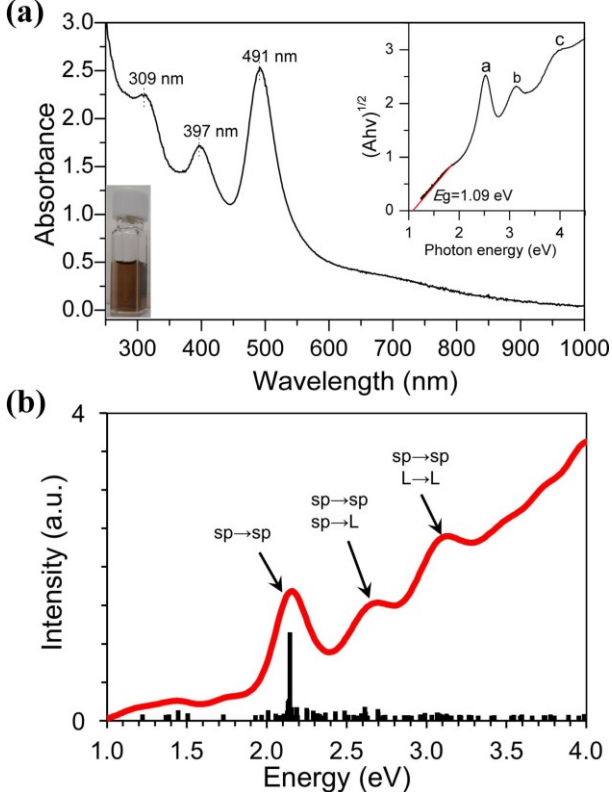


Figure 4. (a) The ultraviolet–visible absorption spectrum of crystals dissolved in CH_2Cl_2 . Inset (left bottom): Photograph showing the CH_2Cl_2 solution of **SD/Ag48**. Inset (right top): the spectrum on the energy scale (eV). (b) Calculated absorption spectrum for $Ag_{48}(CrO_4)_7(HC\equiv C)_{20}$. The 200 excited states with the largest oscillator strength are shown as stick spectra. In the calculated spectra, sp denotes MOs that originate mainly from delocalized Ag s+p orbitals in the Ag_{23} core of the cluster. In comparison, L denotes MOs that have mainly ligand (C p, O p or Cr d) character.

Due to the neutral nature of **SD/Ag48**, the number of valence electrons for the cluster can be calculated to be 14, which is not a spherical magic number for the superatom model.²⁹ Its stability may be explained by a nonspherical kernel geometry³⁰ and

the special coordination effect of surface CrO₄²⁻ anions. To better understand the electronic structure of SD/Ag48, we performed density functional theory (DFT) calculations. All calculations were performed using the ADF2017 package.31 We employed the PBE³² functional with a TZP basis set using the frozen core (FC) approximation for the core electrons (FC freezes 4p electrons and lower shells for Ag, 3p electrons and lower shells for Cr, and 1s electrons for C and O). Scalar relativistic effects were treated using the ZORA Hamiltonian.³³ For simplicity in the analysis of the electronic structure and the nature of excited states, [Ag₄₈(CrO₄)₇('BuC≡C)₂₀] is modelled as [Ag₄₈(CrO₄)₇(HC≡C)₂₀]; however, a comparison of calculated spectra between the two systems is given in Figure S8a. All nanoclusters are calculated using a neutral charge state. In our analysis of electronic structure, molecular orbitals (MOs) are denoted using cylindrical symmetry $(\Sigma, \Pi, \Delta,...)^{34}$ In this nomenclature, MOs are labelled as NM_I, where M corresponds to Σ , Π , Δ , ..., l corresponds to the axial quantum number, and N corresponds to the principal quantum number (N = 1, 2, 3, ...). For the calculation of excited states, we have employed the TD-DFT+TB formalism, 35 which is an approximate time-dependent DFT (TD-DFT) method. For this system, the TD-DFT+TB and TD-DFT methods show excellent agreement for calculated spectra at the PBE/DZ level of theory as shown in Figure S8b.

The electronic structure of the [Ag₄₈(CrO₄)₇(HC≡C)₂₀] cluster can be analyzed by treating the Ag₂₃ core in the structure as a nanorod as shown in Figure 2c, similar to the case of the Au₃₈(SH)₂₄ cluster. ³⁴ As a result, delocalized levels in the electronic structure of [Ag₄₈(CrO₄)₇(HC≡C)₂₀], which mainly originate from Ag s and p levels, exhibit Σ , Π , Δ , ... symmetries. predicted HOMO-LUMO gap [Ag₄₈(CrO₄)₇(HC≡C)₂₀] cluster is 1.05 eV at the PBE/TZP level of theory. Similar to Au₃₈(SH)₂₄, ³⁴ electron counting rules show 14 delocalized electrons in the neutral $[Ag_{48}(CrO_4)_7(HC \equiv C)_{20}]$ as well. In the calculated electronic structure, the HOMO, HOMO-1 and HOMO-2 levels dominantly originate from Ag s and p levels of the Ag₂₃ core. The HOMO level shows Σ_3 symmetry, whereas the HOMO-1 and HOMO-2 levels exhibit Π_2 symmetry. In the unoccupied levels, the LUMO and LUMO+1 show Π and Δ character respectively; however, they also have large contributions from Cr d and O p orbitals. In fact, from the LUMO to LUMO+17 levels, the MOs generally exhibit mixing between the Σ , Π and Δ levels that originate from the Ag₂₃ core, and the Cr d and O p orbitals.

In Figure 4, we show a comparison of the experimental UV-vis spectra, and the calculated absorption spectra for $[Ag_{48}(CrO_4)_7(HC\equiv C)_{20}]$ (Figure 4b). In general, there is a very good agreement between the calculated and experimental spectra, especially for the spectral shape. Both spectra exhibit three distinct features in the 2-4 eV region. In particular, an intense feature (peak a) is seen at 2.5 eV in the experimental spectra, which is also predicted in the calculated spectra at 2.15 eV. The predicted energies of the peaks are generally redshifted in the calculated spectra by 0.3-0.8 eV compared to the experimental spectra. This redshift is commonly seen for predicted absorption spectra of ligand-protected gold and silver clusters when GGA functionals are employed in the computation.³⁶

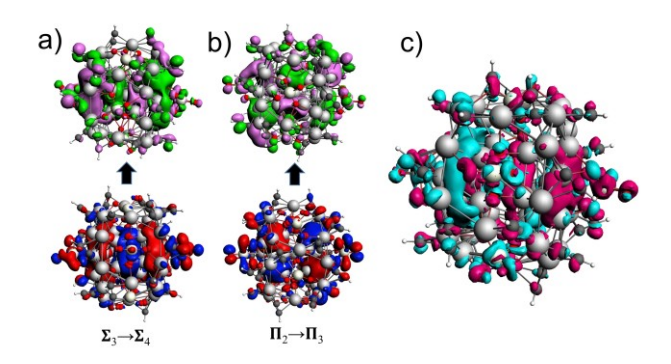


Figure 5. Occupied-unoccupied orbitals for a) the $\Sigma_3 \rightarrow \Sigma_4$ transition and b) the $\Pi_2 \rightarrow \Pi_3$ transition that contribute significantly to peak a in Figure 4a. The oscillator strength contribution from the $\Sigma_3 \rightarrow \Sigma_4$ transition is ~2 times larger than the oscillator strength contribution of the $\Pi_2 \rightarrow \Pi_3$ transition. c) The calculated transition-fit density is shown for the excited state at 2.15 eV (corresponding to peak a in Figure 4a), which has the largest oscillator strength among the calculated excited states.

In the calculated spectra, the strong feature at 2.15 eV (peak a) is predicted to arise mainly from HOMO->LUMO+16 $(\Sigma_3 \rightarrow \Sigma_4)$ and HOMO-1 \rightarrow LUMO+15 $(\Pi_2 \rightarrow \Pi_3)$ transitions as shown in Figure 5a and 5b respectively. The nature of the transitions is similar to the intense longitudinal transitions in nanorods³⁷ where $\Delta M=0$ and $\Delta l=\pm 1$. As expected from the nature of MOs involved, the calculated transition-fit density exhibits a large polarization along the long axis of the Ag₂₃ core as shown in Figure 5c, corresponding to a strong dipolar excitation. In comparison, peak b and peak c are predicted to originate from a large number of lower oscillator strength states. Peak b mainly arises from transitions out of occupied HOMO-HOMO-2 levels to higher-lying unoccupied Σ and Π levels and ligand-based unoccupied orbitals that have dominantly C p and Cr d character. In the case of peak c, the largest contribution to the peak's oscillator strength comes from the HOMO-9→LUMO+17 $(\Pi_1 \rightarrow 2\Sigma_1)$ transition. Additionally, transitions between ligandbased levels and the Ag d band also contribute considerably to the oscillator strength of this peak.

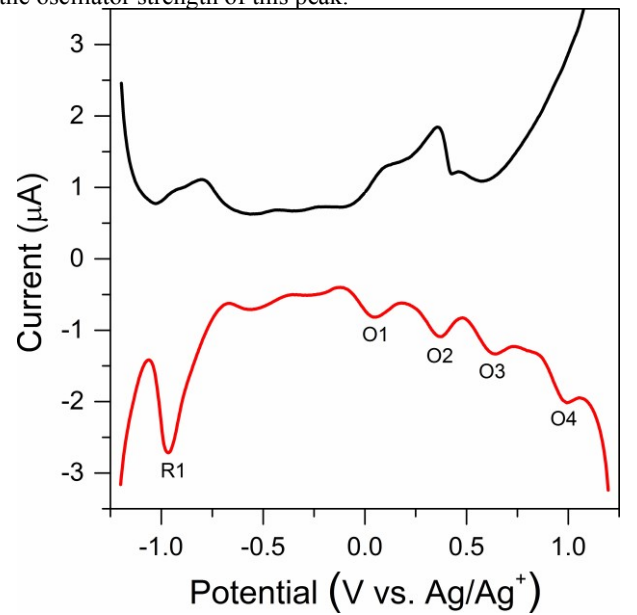


Figure 6. Differential pulse voltammogram of SD/Ag48 at room temperature

Electrochemistry of SD/Ag48

Electrochemistry is a powerful technique widely used to investigate the electronic energy structure of metal nanoclusters near to the HOMO-LUMO levels.³⁸ To study the electrochemical property of **SD/Ag48**, we carried out cyclic voltammetry (CV, Figure S9) and differential pulse voltammetry (DPV) of **SD/Ag48** at room temperature in 0.1 M CH₂Cl₂ solution of ⁿBu₄NPF₆. The scan direction is from 1.0 V to –1.0 V, and then back from –1.0 to 1.0 V. As shown in Figure 6, there are four oxidation peaks at 0.05 (O1), 0.37 (O2), 0.64 (O3) and 0.99 V (O5) and one reduction peak at –0.97 V (R1). The electrochemical gap deduced from the difference between the first oxidation (O1) and reduction (R1) potentials gives an energy of 1.02 eV,³⁹ which is well matched with the experimental (1.09 eV) and calculated HOMO-LUMO gap value (1.05 eV) at the PBE/TZP level for **SD/Ag48**.

Luminescence of SD/Ag48

The luminescence properties of the **SD/Ag48** were studied in solid state and CH_2Cl_2 solution. It was non-emissive in the solid state at room temperature, even at cryogenic temperature. In CH_2Cl_2 solution, **SD/Ag48** exhibits an emission peak at 420 nm ($\lambda_{ex} = 288$ nm) at room temperature (Figure 7), whereas the maximum emission peak red-shifts to 441 nm in frozen CH_2Cl_2 glass with a lifetime falling microsecond scale ($\tau_1 = 0.28$ and $\tau_2 = 6.54$ µs; Figure S10) at 80 K. Based on the previous reports about the luminescence of silver clusters, ^{25d, 40} the luminescence excited state of **SD/Ag48** can be tentatively ascribed to a combination of ligand-to-metal charge transfer (LMCT) and metal-centered (MC) transitions influenced by argentophilic interactions. ⁴¹

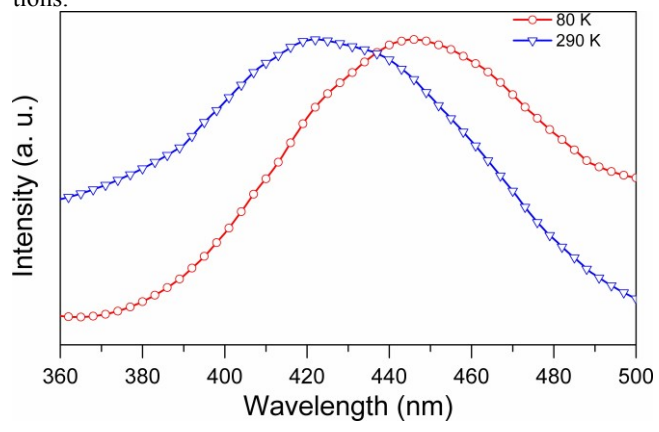


Figure 7. The normalized luminescent spectra of **SD/Ag48** recorded in CH₂Cl₂ solution at 80 to 290 K under the excitation of 288 nm.

CONCLUSIONS

In summary, this work presents a novel silver nanocluster coprotected by organic ${}^{\prime}BuC\equiv C^{-}$ ligands and inorganic $CrO_4{}^{2-}$ anions for the first time. The SD/Ag48 shows a double-shell structure with a rare Ino decahedral Ag_{23} kernel protected by an outer drum-like Ag_{25} shell. The inorganic oxo protecting ligands play three important roles: i) passivating the Ag_{23} kernel; ii) connecting the core and shell; and iii) protecting the Ag_{25} shell, in the construction of SD/Ag48, and partially contribute to its optical properties. The structural, optical and electronic properties of the cluster are also investigated by theoretical methods. These results show that the strong optical peak at 2.5 eV arises from

an excitation that is polarized along the long axis of the Ag₂₃ core. Optical spectroscopy, electrochemistry, and DFT calculations predict a HOMO-LUMO gap around 1.0-1.1 eV. The nanocluster also has visible luminescence in solution. We believe that this work will open a fresh avenue in the construction of new silver nanoclusters by the combination of organic ligands and inorganic oxo anions. Further work on modulating the structures of silver nanocluster by introducing different inorganic oxo anions is in progress.

ASSOCIATED CONTENT

Supporting Information. Experimental details, detailed crystallographic structure and data including the CIF file, PXRD, IR, EDS mapping. This information is available free of charge via the internet at http://pubs.acs.org.

AUTHOR INFORMATION

Corresponding Author

cmaikens@ksu.edu

dsun@sdu.edu.cn

ORCID

Di Sun: 0000-0001-5966-1207

Christine Aikens: 0000-0002-0854-7997

Notes

The authors declare no competing financial interest.

ACKNOWLEDGMENT

This work was financially supported by the National Natural Science Foundation of China (Grant Nos. 21822107, 21571115, 21701133, 21827801), the Natural Science Foundation of Shandong Province (Nos. JQ201803 and ZR2017MB061), the Taishan Scholar Project of Shandong Province of China, the Qilu Youth Scholar Funding of Shandong University and the Fundamental Research Funds of Shandong University (104.205.2.5). F.A. and C.M.A were supported by the National Science Foundation (CHE-1507909) of the United States. The computing for this work was performed on the Beocat Research Cluster at Kansas State University, which is funded in part by NSF grants CHE-1726332, CNS-1006860, EPS-1006860, and EPS-0919443.

REFERENCES

- (a) Lei, Z.; Wan, X. K.; Yuan, S. F.; Guan, Z. J.; Wang, Q. M. Alkynyl Approach toward the Protection of Metal Nanoclusters. *Acc. Chem. Res.* 2018, 51 (10), 2465-2474. (b) Sharma, S.; Chakrahari, K. K.; Saillard, J. Y.; Liu, C. W. Structurally Precise Dichalcogenolate-Protected Copper and Silver Superatomic Nanoclusters and Their Alloys. *Acc. Chem. Res.* 2018, 51 (10), 2475-2483. (c) Yao, Q. F.; Chen, T. K.; Yuan, X.; Xie, J. P. Toward Total Synthesis of Thiolate-Protected Metal Nanoclusters. *Acc. Chem. Res.* 2018, 51 (6), 1338-1348. (d) Konishi, K. In *Gold Clusters, Colloids and Nanoparticles I*, Mingos, D. M. P., Ed., 2014, 49-86.
- (2) Wang, Y.; Zheng, Y. Q.; Huang, C. Z.; Xia, Y. N. Synthesis of Ag Nanocubes 18-32 nm in Edge Length: The Effects of Polyol on Reduction Kinetics, Size Control, and Reproducibility. *J. Am. Chem.* Soc. 2013, 135 (5), 1941-1951.

- (3) Jadzinsky, P. D.; Calero, G.; Ackerson, C. J.; Bushnell, D. A.; Kornberg, R. D. Structure of a Thiol Monolayer-Protected Gold Nanoparticle at 1.1 Angstrom Resolution. *Science* 2007, 318 (5849), 430-433.
- (a) Zhu, M.; Aikens, C. M.; Hollander, F. J.; Schatz, G. C.; Jin, R. Correlating the Crystal Structure of a Thiol-Protected Au₂₅ Cluster and Optical Properties. J. Am. Chem. Soc. 2008, 130 (18), 5883-5885. (b) Das, A.; Li, T.; Nobusada, K.; Zeng, Q.; Rosi, N. L.; Jin, R. C. Total Structure and Optical Properties of A Phosphine/Thiolate-Protected Au₂₄ Nanocluster. J. Am. Chem. Soc. 2012, 134 (50), 20286-20289. (c) Das, A.; Li, T.; Nobusada, K.; Zeng, C. J.; Rosi, N. L.; Jin, R. C. Nonsuperatomic [Au₂₃(SC₆H₁₁)₁₆] Nanocluster Featuring Bipyramidal Au₁₅ Kernel and Trimeric Au₃(SR)₄ Motif. J. Am. Chem. Soc. 2013, 135 (49), 18264-18267. (d) Kamei, Y.; Shichibu, Y.; Konishi, K. Generation of Small Gold Clusters with Unique Geometries through Cluster-to-Cluster Transformations: Octanuclear Clusters with Edge-sharing Gold Tetrahedron Motifs. Angew. Chem., Int. Edit. 2011, 50 (32), 7442-7445. (e) Sugiuchi, M.; Shichibu, Y.; Konishi, K. An Inherently Chiral Au₂₄ Framework with Double-Helical Hexagold Strands. Angew. Chem., Int. Edit. 2018, 57 (26), 7855-7859. (f) Shichibu, Y.; Zhang, M.; Kamei, Y.; Konishi, K. [Au₇]³⁺: A Missing Link in the Four-Electron Gold Cluster Family. J. Am. Chem. Soc. 2014, 136 (37), 12892-12895. (g) Abu Bakar, M.; Sugiuchi, M.; Iwasaki, M.; Shichibu, Y.; Konishi, K. Hydrogen Bonds to Au Atoms in Coordinated Gold Clusters. Nat. Commun. 2017, 8, 576. (h) Kurashige, W.; Niihori, Y.; Sharma, S.; Negishi, Y. Precise Synthesis, Functionalization and Application of Thiolate-Protected Gold Clusters. Coord. Chem. Rev. 2016, 320, 238-250. (i) Yao, L.-Y.; Yam, V. W.-W. Diphosphine-Stabilized Small Gold Nanoclusters: From Crystal Structure Determination to Ligation-Driven Symmetry Breaking and Anion Exchange Properties. J. Am. Chem. Soc. 2016, 138 (48), 15736-15742. (j) Chen, J.; Zhang, Q.-F.; Bonaccorso, T. A.; Williard, P. G.; Wang, L.-S. Controlling Gold Nanoclusters by Diphospine Ligands. J. Am. Chem. Soc. 2014, 136 (1), 92-95. (k) Liao, L.; Zhuang, S.; Wang, P.; Xu, Y.; Yan, N.; Dong, H.; Wang, C.; Zhao, Y.; Xia, N.; Li, J.; Deng, H.; Pei, Y.; Tian, S.-K.; Wu, Z. Quasi-Dual-Packed-Kerneled Au₄₉(2,4-DMBT)₂₇ Nanoclusters and the Influence of Kernel Packing on the Electrochemical Gap. Angew. Chem., Int. Ed. 2017, 56 (41), 12644-12648. (l) Wu, Z. Anti-Galvanic Reduction of Thiolate-Protected Gold and Silver Nanoparticles. Angew. Chem., Int. Ed. 2012, 51 (12), 2934-2938.
- (5) Zeng, C. J.; Chen, Y. X.; Kirschbaum, K.; Lambright, K. J.; Jin, R. C. Emergence of Hierarchical Structural Complexities in Nanoparticles and Their Assembly. *Science* 2016, 354 (6319), 1580-1584.
- (6) Dhayal, R. S.; Liao, J.-H.; Liu, Y.-C.; Chiang, M.-H.; Kahlal, S.; Saillard, J.-Y.; Liu, C. W. [Ag₂₁{S₂P(OiPr)₂}₁₂]⁺: An Eight-Electron Superatom. *Angew. Chem., Int. Edit.* 2015, 54 (12), 3702-3706.
- (7) Liu, C.; Li, T.; Abroshan, H.; Li, Z. M.; Zhang, C.; Kim, H. J.; Li, G.; Jin, R. C. Chiral Ag₂₃ Nanocluster with Open Shell Electronic Structure and Helical Face-Centered Cubic Framework. *Nat. Commun.* 2018, 9, 744.
- (8) Joshi, C. P.; Bootharaju, M. S.; Alhilaly, M. J.; Bakr, O. M., [Ag₂₅(SR)₁₈]⁻: The "Golden" Silver Nanoparticle. *J. Am. Chem. Soc.* 2015, 137 (36), 11578-11581.
- (9) AbdulHalim, L. G.; Bootharaju, M. S.; Tang, Q.; Del Gobbo, S.; AbdulHalim, R. G.; Eddaoudi, M.; Jiang, D.-e.; Bakr, O. M. Ag₂₉(BDT)₁₂(TPP)₄: A Tetravalent Nanocluster. *J. Am. Chem. Soc.* 2015, *137* (37), 11970-11975.
- (10) Sun, D.; Luo, G.-G.; Zhang, N.; Huang, R.-B.; Zheng, L.-S. Simultaneous Self-Assembly of A Cage-like Silver(I) Complex Encapsulating An Ag₆ Neutral Cluster Core and Carbon Dioxide Fixation. *Chem. Commun.* 2011, 47 (5), 1461-1463.
- (11) (a) Yang, H.; Wang, Y.; Huang, H.; Gell, L.; Lehtovaara, L.; Malola, S.; Häkkinen, H.; Zheng, N. All-Thiol-Stabilized Ag₄₄ and Au₁₂Ag₃₂ Nanoparticles with Single-Crystal Structures. *Nat. Commun.* 2013, 4, 2422. (b) Desireddy, A.; Conn, B. E.; Guo, J.; Yoon, B.; Barnett, R. N.; Monahan, B. M.; Kirschbaum, K.; Griffith, W. P.; Whetten, R. L.; Landman, U.; Bigioni, T. P. Ultrastable Silver Nanoparticles. *Nature* 2013, 501, 399-402.

- (12) Chai, J. S.; Yang, S.; Lv, Y.; Chen, T.; Wang, S. X.; Yu, H. Z.; Zhu, M.-Z. A Unique Pair: Ag₄₀ and Ag₄₆ Nanoclusters with the Same Surface but Different Cores for Structure-Property Correlation. *J. Am. Chem. Soc.* 2018, 140 (46), 15582-15585.
- (13) Du, W. J.; Jin, S.; Xiong, L.; Chen, M.; Zhang, J.; Zou, X. J.; Pei, Y.; Wang, S. X.; Zhu, M. Z. Ag₅₀(Dppm)₆(SR)₃₀ and Its Homologue Au_xAg_{50-x}(Dppm)₆(SR)₃₀ Alloy Nanocluster: Seeded Growth, Structure Determination, and Differences in Properties. *J. Am. Chem. Soc.* 2017, 139 (4), 1618-1624.
- (14) Jin, S.; Wang, S. X.; Song, Y. B.; Zhou, M.; Zhong, J.; Zhang, J.; Xia, A. D.; Pei, Y.; Chen, M.; Li, P.; Zhu, M.-Z. Crystal Structure and Optical Properties of the [Ag₆₂S₁₂(SBu¹)₃₂]²⁺ Nanocluster with a Complete Face-Centered Cubic Kernel. *J. Am. Chem. Soc.* 2014, 136 (44), 15559-15565.
- (15) Alhilaly, M. J.; Bootharaju, M. S.; Joshi, C. P.; Besong, T. M.; Emwas, A.-H.; Juarez-Mosqueda, R.; Kaappa, S.; Malola, S.; Adil, K.; Shkurenko, A.; Hakkinen, H.; Eddaoudi, M.; Bakr, O. M. [Ag₆₇(SPhMe₂)₃₂(PPh₃)₈]³⁺: Synthesis, Total Structure, and Optical Properties of a Large Box-Shaped Silver Nanocluster. *J. Am. Chem. Soc.* 2016, *138* (44), 14727-14732.
- (16) Qu, M.; Li, H.; Xie, L. H.; Yan, S. T.; Li, J. R.; Wang, J. H.; Wei, C. Y.; Wu, Y. W.; Zhang, X. M. Bidentate Phosphine-Assisted Synthesis of an All-Alkynyl-Protected Ag₇₄ Nanocluster. *J. Am. Chem. Soc.* 2017, *139* (36), 12346-12349
- (17) Ren, L.; Yuan, P.; Su, H.; Malola, S.; Lin, S.; Tang, Z.; Teo, B. K.; Hakkinen, H.; Zheng, L.; Zheng, N. Bulky Surface Ligands Promote Surface Reactivities of [Ag₁₄₁X₁₂(S-Adm)₄₀]³⁺ (X = Cl, Br, I) Nanoclusters: Models for Multiple-Twinned Nanoparticles. *J. Am. Chem. Soc.* 2017, *139* (38), 13288-13291.
- (18) Song, Y. B.; Lambright, K.; Zhou, M.; Kirschbaum, K.; Xiang, J.; Xia, A. D.; Zhu, M.-Z.; Jin, R. C. Large-Scale Synthesis, Crystal Structure, and Optical Properties of the Ag₁₄₆Br₂(SR)₈₀ Nanocluster. ACS Nano. 2018, 12 (9), 9318-9325.
- (19) Yan, J. Z.; Zhang, J.; Chen, X. M.; Malola, S.; Zhou, B.; Selenius, E.; Zhang, X. M.; Yuan, P.; Deng, G. C.; Liu, K. L.; Su, H. F.; Teo, B. K.; Häkkinen, H.; Zheng, L. S.; Zheng, N. F. Thiol-Stabilized Atomically Precise, Superatomic Silver Nanoparticles for Catalysing Cycloisomerization of Alkynyl Amines. *Natl. Sci. Rev.* 2018, 5(5), 694-702.
- (20) Liu, J. Y.; Alkan, F.; Wang, Z.; Zhang, Z. Y.; Kurmoo, M.; Yan, Z.; Zhao, Q. Q.; Aikens, C. M.; Tung, C. H.; Sun, D. Different Silver Nanoparticles in One Crystal: Ag₂₁₀(*i*PrPhS)₇₁(Ph₃P)₆Cl and Ag₂₁₁(*i*PrPhS)₇₁(Ph₃P)₆Cl, Angew. Chem., Int. Ed. 2019, 58, 195-199
- (21) Yang, H. Y.; Wang, Y.; Chen, X.; Zhao, X. J.; Gu, L.; Huang, H. Q.; Yan, J. Z.; Xu, C. F.; Li, G.; Wu, J. C.; Edwards, A. J.; Dittrich, B.; Tang, Z. C.; Wang, D. D.; Lehtovaara, L.; Hakkinen, H.; Zheng, N. F. Plasmonic Twinned Silver Nanoparticles With Molecular Precision. *Nat. Commun.* 2016, 7, 12809.
- (22) (a) Liu, P.; Qin, R.; Fu, G.; Zheng, N. Surface Coordination Chemistry of Metal Nanomaterials. J. Am. Chem. Soc. 2017, 139 (6), 2122-2131. (b) Hakkinen, H. The Gold-Sulfur Interface at the Nanoscale. Nat. Chem. 2012, 4 (6), 443-455.
- (23) (a) Crasto, D.; Malola, S.; Brosofsky, G.; Dass, A.; Hakkinen, H. Single Crystal XRD Structure and Theoretical Analysis of the Chiral Au₃₀S(S-t-Bu)₁₈ Cluster. J. Am. Chem. Soc. 2014, 136 (13), 5000-5005. (b) Shichibu, Y.; Konishi, K., HCl-Induced Nuclearity Convergence in Diphosphine-Protected Ultrasmall Gold Clusters: A Novel Synthetic Route to "Magic-Number" Au₁₃ Clusters. Small 2010, 6 (11), 1216-1220.
- (24) (a) Liu, J.-W.; Feng, L.; Su, H.-F.; Wang, Z.; Zhao, Q.-Q.; Wang, X.-P.; Tung, C.-H.; Sun, D.; Zheng, L.-S. Anisotropic Assembly of Ag₅₂ and Ag₇₆ Nanoclusters. *J. Am. Chem. Soc.* 2018, *140*, 1600-1603. (b) Wang, Z.; Su, H.-F.; Kurmoo, M.; Tung, C.-H.; Sun, D.; Zheng, L.-S. Trapping An Octahedral Ag₆ Kernel in A Seven-Fold Symmetric Ag₅₆ Nanowheel. *Nat. Commun.* 2018, *9*, 2094. (c) Wang, Z.; Su, H.-F.; Tung, C.-H.; Sun, D.; Zheng, L.-S. Deciphering Synergetic Coreshell Transformation from [Mo₆O₂₂@Ag₄₄] to [Mo₈O₂₈@Ag₅₀]. *Nat. Commun.* 2018, *9*, 4407.
- (25) (a) Schmidbaur, H.; Schier, A. Argentophilic Interactions. *Angew. Chem., Int. Ed.* 2015, 54 (3), 746-784. (b) Wang, Z.-Y.; Wang, M.-Q.; Li, Y.-L.; Luo, P.; Jia, T.-T.; Huang, R.-W.; Zang, S.-Q.; Mak,

- T. C. W. Atomically Precise Site-Specific Tailoring and Directional Assembly of Superatomic Silver Nanoclusters. *J. Am. Chem. Soc.* **2018**, *140* (3), 1069-1076. (c) Duan, G. X.; Tian, L.; Wen, J. B.; Li, L. Y.; Xie, Y. P.; Lu, X. An Atomically Precise All-Tert-Butylethynide-protected Ag₅₁ Superatom Nanocluster with Color Tunability. *Nanoscale* **2018**, *10* (40), 18915-18919. (d) Huang, R.-W.; Wei, Y.-S.; Dong, X.-Y.; Wu, X.-H.; Du, C.-X.; Zang, S.-Q.; Mak, T. C. W. Hypersensitive Dual-Function Luminescence Switching of A Silver-Chalcogenolate Cluster-based Metal-Organic Framework. *Nat. Chem.* **2017**, *9* (7), 689-697.
- (26) Jin, R. C.; Zeng, C. J.; Zhou, M.; Chen, Y. X. Atomically Precise Colloidal Metal Nanoclusters and Nanoparticles: Fundamentals and Opportunities. *Chem. Rev.* 2016, 116 (18), 10346-10413.
- (27) (a) Yuan, S. F.; Li, P.; Tang, Q.; Wan, X. K.; Nan, Z. A.; Jiang, D. E.; Wang, Q. M. Alkynyl-Protected Silver Nanoclusters Featuring An Anticuboctahedral Kernel. *Nanoscale* 2017, 9 (32), 11405-11409. (b) Guan, Z.-J.; Zeng, J.-L.; Nan, Z.-A.; Wan, X.-K.; Lin, Y.-M.; Wang, Q.-M. Thiacalix[4]arene: New Protection for Metal Nanoclusters. *Sci. Adv.* 2016, 2 (8), e1600323.
- (28) Chen, Y. X.; Zeng, C. J.; Liu, C.; Kirschbaum, K.; Gayathri, C.; Gil, R. R.; Rosi, N. L.; Jin, R. C. Crystal Structure of Barrel-Shaped Chiral Au₁₃₀(p-MBT)₅₀ Nanocluster. *J. Am. Chem. Soc.* 2015, *137* (32), 10076-10079.
- (29) (a) Hakkinen, H. Atomic and Electronic Structure of Gold Clusters: Understanding Flakes, Cages and Superatoms from Simple Concepts. *Chem. Soc. Rev.* 2008, 37 (9), 1847-1859. (b) Walter, M.; Akola, J.; Lopez-Acevedo, O.; Jadzinsky, P. D.; Calero, G.; Ackerson, C. J.; Whetten, R. L.; Groenbeck, H.; Hakkinen, H. A Unified View of Ligand-Protected Gold Clusters as Superatom Complexes. *PNAS* 2008, 105 (27), 9157-9162.
- (30) Fernando, A.; Dimuthu, K. L.; Weerawardene, M.; Karimova, N. V.; Aikens, C. M. Quantum Mechanical Studies of Large Metal, Metal Oxide, and Metal Chalcogenide Nanoparticles and Clusters. *Chem. Rev.* **2015**, *115* (12), 6112-6216.
- (31) (a) ADF2017, SCM, Theoretical Chemistry, Vrije Universiteit, Amsterdam, The Netherlands, http://www.scm.com/. (b) Guerra, C. F.; Snijders, J. G.; te Velde, G.; Baerends, E. J. Towards An Order-N DFT Method. *Theor. Chem. Acc.* 1998, 99 (6), 391-403. (c) te Velde, G.; Bickelhaupt, F. M.; Baerends, E. J.; Guerra, C. F.; Van Gisbergen, S. J. A.; Snijders, J. G.; Ziegler, T. Chemistry with ADF. *J. Comput. Chem.* 2001, 22 (9), 931-967.
- (32) (a) Perdew, J. P.; Burke, K.; Ernzerhof, M. Generalized Gradient Approximation made Simple. *Phys. Rev. Lett.* 1996, 77 (18), 3865-3868.

- (b) Perdew, J. P.; Burke, K.; Wang, Y. Generalized Gradient Approximation for the Exchange-Correlation Hole of A Many-Electron System. *Phys. Rev. B* **1996**, *54* (23), 16533-16539.
- (33) (a) Lenthe, E. v.; Baerends, E. J.; Snijders, J. G. Relativistic Total Energy using Regular Approximations. J. Chem. Phys. 1994, 101 (11), 9783-9792. (b) Lenthe, E. v.; Snijders, J. G.; Baerends, E. J. The Zero-Order Regular Approximation for Relativistic Effects: The Effect of Spin-Orbit Coupling in Closed Shell Molecules. J. Chem. Phys. 1996, 105 (15), 6505-6516.
- (34) Lopez-Acevedo, O.; Tsunoyama, H.; Tsukuda, T.; Hakkinen, H.; Aikens, C. M. Chirality and Electronic Structure of the Thiolate-Protected Au₃₈ Nanocluster. *J. Am. Chem. Soc.* 2010, *132* (23), 8210-8218.
- (35) Ruger, R.; van Lenthe, E.; Heine, T.; Visscher, L. Tight-Binding Approximations to Time-Dependent Density Functional Theory-A Fast Approach for the Calculation of Electronically Excited States. *J. Chem. Phys.* 2016, 144 (18), 184103.
- (36) (a) Aikens, C. M. Effects of Core Distances, Solvent, Ligand, and Level of Theory on the TDDFT Optical Absorption Spectrum of the Thiolate-Protected Au₂₅ Nanoparticle. J. Phys. Chem. A 2009, 113 (40), 10811-10817. (b) Fernando, A.; Dimuthu, K. L.; Weerawardene, M.; Karimova, N. V.; Aikens, C. M. Quantum Mechanical Studies of Large Metal, Metal Oxide, and Metal Chalcogenide Nanoparticles and Clusters. Chem. Rev. 2015, 115 (12), 6112-6216.
- (37) (a) Johnson, H. E.; Aikens, C. A., Electronic Structure and TDDFT Optical Absorption Spectra of Silver Nanorods. J. Phys. Chem. A 2009, 113 (16), 4445-4450. (b) Guidez, E. B.; Aikens, C. M. Diameter Dependence of the Excitation Spectra of Silver and Gold Nanorods. J. Phys. Chem. C 2013, 117 (23), 12325-12336.
- (38) Kwak, K.; Tang, Q.; Kim, M.; Jiang, D.-e.; Lee, D. Interconversion between Superatomic 6-Electron and 8-Electron Configurations of M@Au₂₄(SR)₁₈ Clusters (M = Pd, Pt). J. Am. Chem. Soc. 2015, 137 (33), 10833–10840.
- (39) Kwak, K.; Lee, D. Electrochemical Characterization of Water-Soluble Au₂₅ Nanoclusters Enabled by Phase-Transfer Reaction. J. Phys. Chem. Lett. 2012, 3 (17), 2476-2481.
- (40) Wu, H. -B.; Huang, Z.-J.; Wang, Q. -M. Unprecedented Solution-Stable Silver(I) Ethynediyl Clusters. Chem. Eur. J. 2010, 16 (41), 12321-12323.
- (41) Yam, V. W.-W.; Au, V. K.-M.; Leung, S. Y.-L. Light-Emitting Self-Assembled Materials Based on d⁸ and d¹⁰ Transition Metal Complexes. *Chem. Rev.* 2015, 115 (15), 7589-7728.

Table of Content

